The Study of Charge Separation in Relativistic Heavy-Ion Collisions

1. Introductions
2. The magnetic fields in Realtivistic HIC
3. Charge Separation in Relativistic HIC
4. Summary and Conclusions

Sheng-Qin Feng（冯笙琴）

Three Gorges University (三峡大学)

1. Introduction

Strong

Strong matter produced in heavy ion collisions

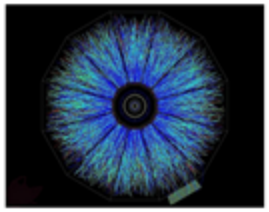

Topological charge changing transitions

induce difference between number of left- and right-handed fermions

Parity to be violated locally in microscopic domains in QCD at finite temperature

ElectroWeak Matter

Electroweak matter produced in the early universe

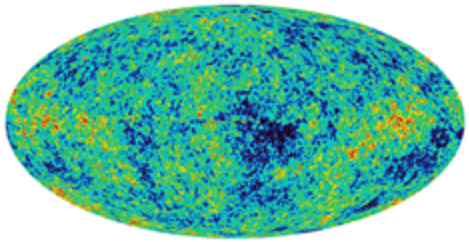

Topological charge changing transitions

induce nonzero baryon + lepton number

Parity to be violated globally of weak interactions of the standard model

At high temperatures these transitions are unsuppressed (Sphalerons)

Manton ('83), Manton and Klinkhamer ('84), Mclerran and Shaposhnikov ('85)

How to observe topological charge changing transitions in hot quark mater?

An asymmetry between matter and antimatter is observed
Kuzmin, Shaposhnikov ('85)

Instantons and Sphaleron

$$Q_w = \frac{g^2}{8\pi^2}\int d^4x\, \vec{E}_a \cdot \vec{B}_a = 0, \pm 1, \pm 2, \ldots.$$

Stable under smooth deformations
Change topological charge vacuum

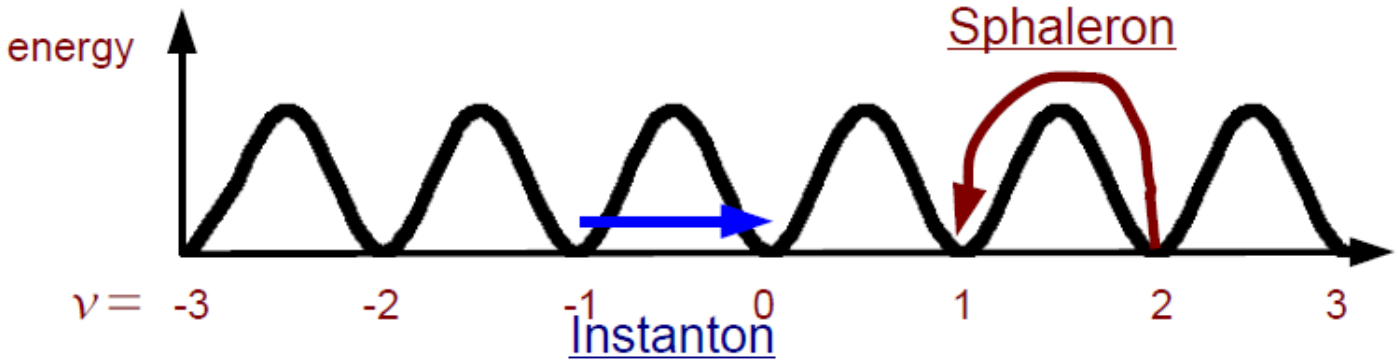

Instantons: Configuration with finite action. **Tunneling through barrier Suppression of rate at T=0,** **'t Hooft ('76), Pisarski and Yaffe ('80)**

Sphaleron: Configuration with finite energy. Go over barrier.

Only possible at finite temperature, rate not suppressed, look for it in QGP!

Manton ('83), Manton and Klinkhamer ('84), McLerran, Mottola and Shaposhnikov ('88)

$$\frac{d N_t^{\pm}}{d^3x\, d\, t} \sim 385\, \alpha_S^5\, T^4$$

Bödeker, Moore and Rummukainen ('00), several transitions per fm^{-3} per fm/c

Use magnetic field to study chirality

A magnetic field will align the spins, depending on their electric charge

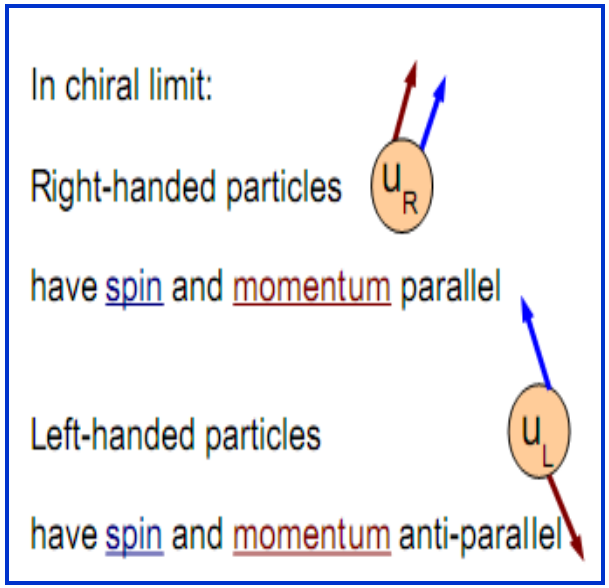

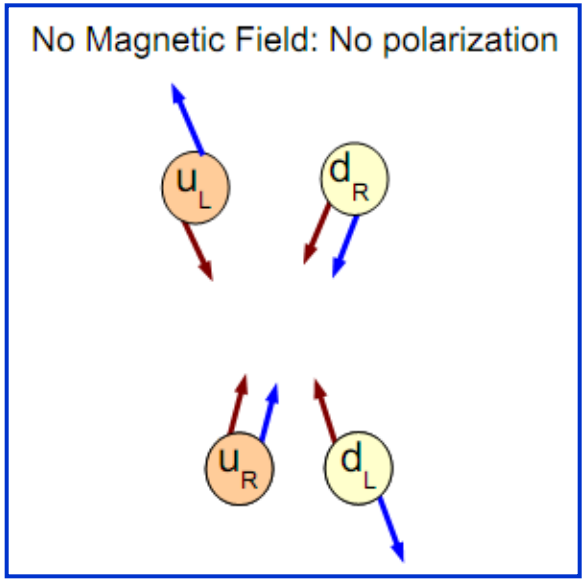

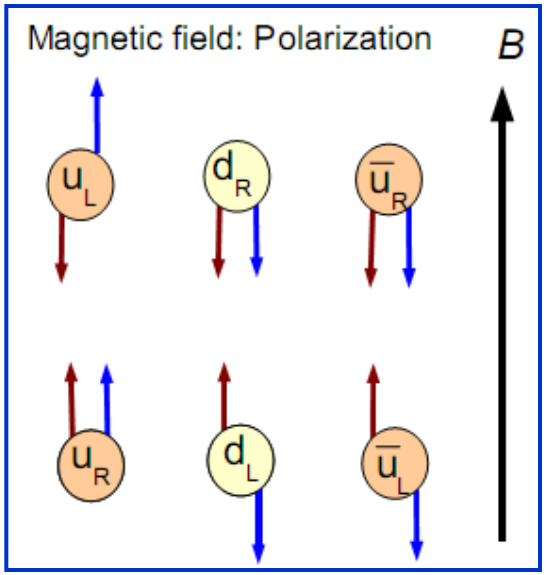

The momenta of the quarks align along the magnetic field

A right-handed up quark will have momentum opposite to a left-handed one

in this way the magnetic field can distinguish between left and right!

D. Kharzeev, L. D. Mclerran, H. J. Warringa, NPA 803, 227 (2008)

The Chiral Magnetic Effect

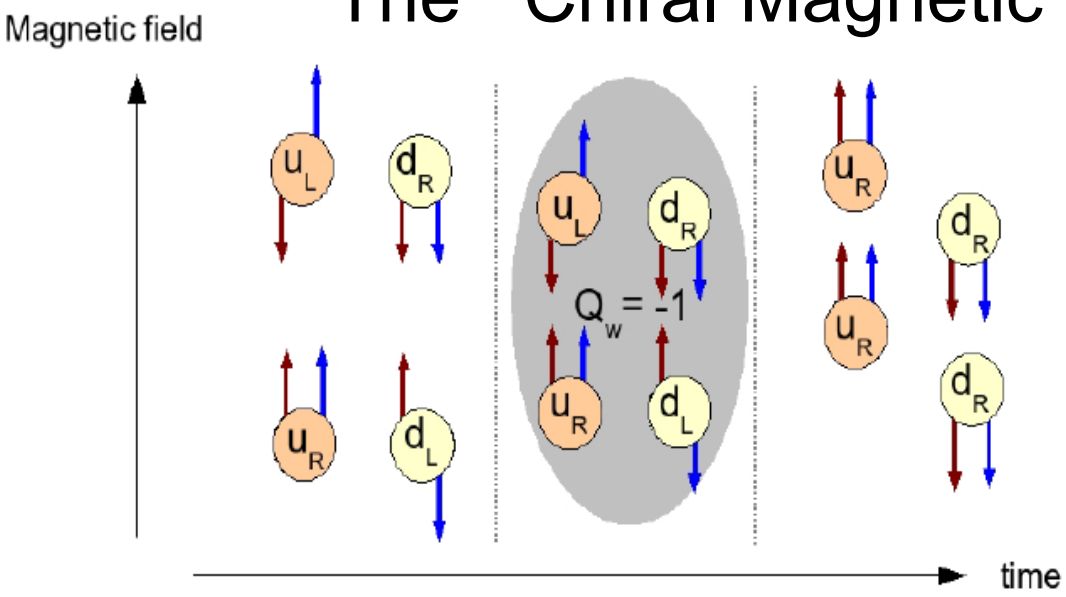

1. Due to very large magnetic field, the up and down quarks in the lowest landau level and can only move along the direction of the magnetic field. Initially there are as many left-handed as right-handed quarks.

2. The quarks interact with a gauge configuration with non-zero Q_w. Assuming Q_w = -1, this will convert a left-handed up/down quark into a right-handed up/down quark by reversing the direction of momentum.

3. The right-handed up quarks will move upwards, the right-handed down quarks will move downwards. A charge of q = 2e will be created between two sides of a plane perpendicular the magnetic fields

In finite volume this causes separation of positive from negative charge

In presence of magnetic field this induces an Electromagnetic Current

D. Kharzeev, L. D. Mclerran, H. J. Warringa, NPA 803, 227 (2008)

The Chiral Magnetic Effect

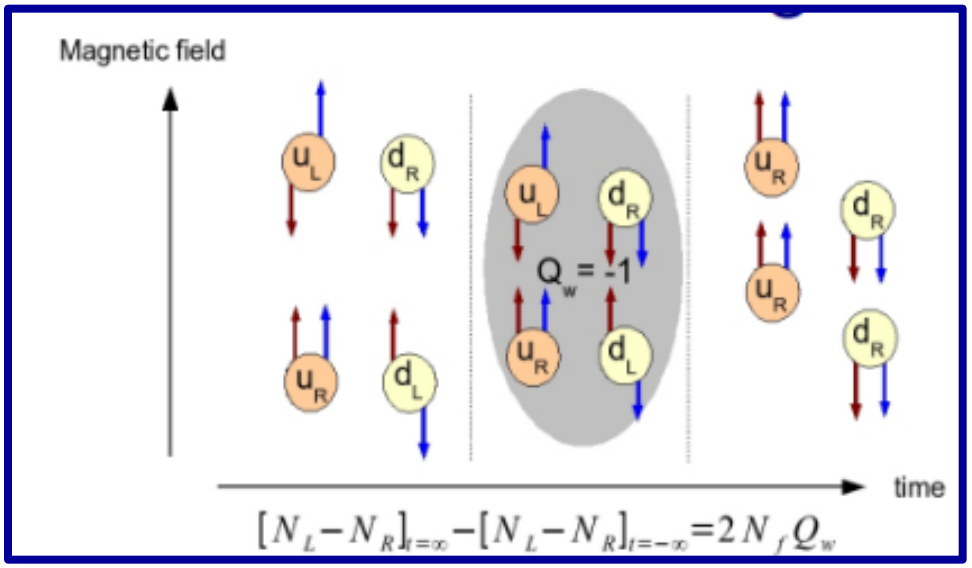

Charge difference:

$$Q = 2 Q_w \sum_f |q_f|$$

Same sign for antiparticles!

Toplogical charge changing transitions induces chirality

In finite volume this causes separation of positive from negative charge

Reasonable polarization of quarks requires:

$$eB \sim \frac{1}{\rho^2} \sim \alpha_s^2 T^2 \sim 10^3 - 10^4 \text{ MeV}^2$$

D. Kharzeev, L. D. Mclerran, H. J. Warringa, NPA 803, 227 (2008)

The Summer School on Frontiers in Theory Physics and the sixth Huada School

2. Magnetic Field in HIC

The Summer School on Frontiers in Theory Physics and the sixth Huada School on QCD, 5.22 - 6.2, Sheng-Qin Feng

Consider the Woods-Saxon nucleon distribution with the thickness of the Lorentz contraction of the nuclear collision in the Z directions

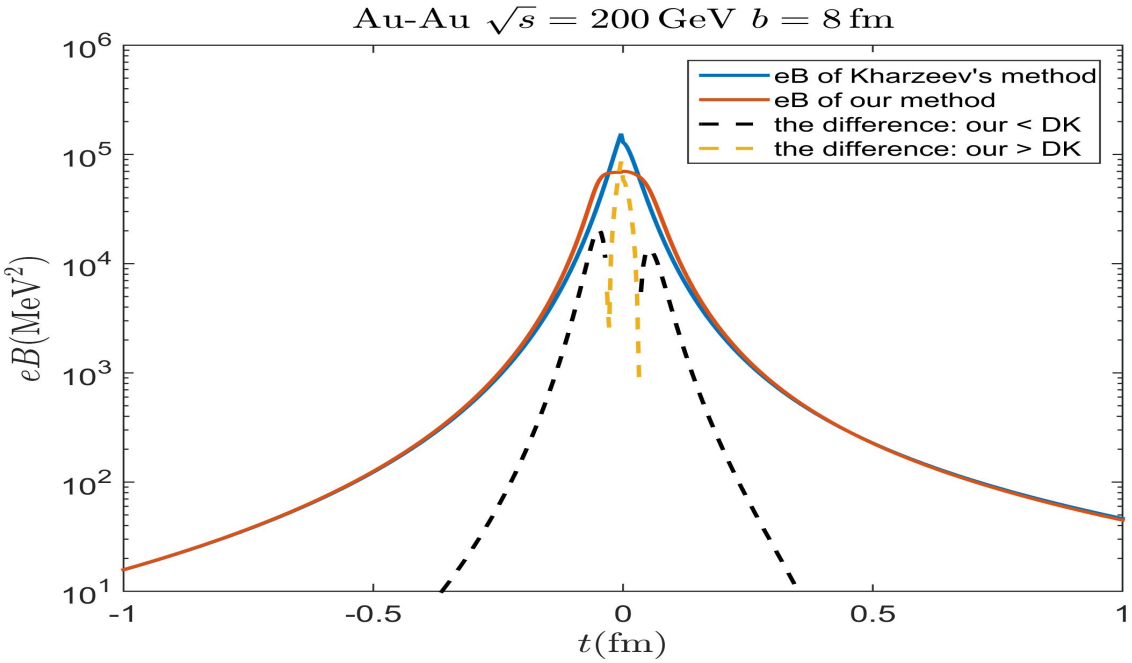

KMW's model --**pancake approximation**

RHIC@BNL

$$eB(\tau = 0.2\,\mathrm{fm}) = 10^3 \sim 10^4\ \mathrm{MeV}^2 \sim 10^{17}\,\mathrm{G}$$

Reasonable polarization of quarks requires: $eB \sim 1/\rho^2 \sim 10^3 - 10^4\ \mathrm{MeV}^2$

Y. J. Mo, S. Q. Feng and Y. F. Shi, Phys. Rev. C 024901 (2013);
X.Ai and S.Q. Feng, College Physics, 2017, to be published.

D. Kharzeev, L. D. Mclerran, H. J. Warringa, NPA 803, 227 (2008)

Magnetic field varies with time in heavy-ion collisions

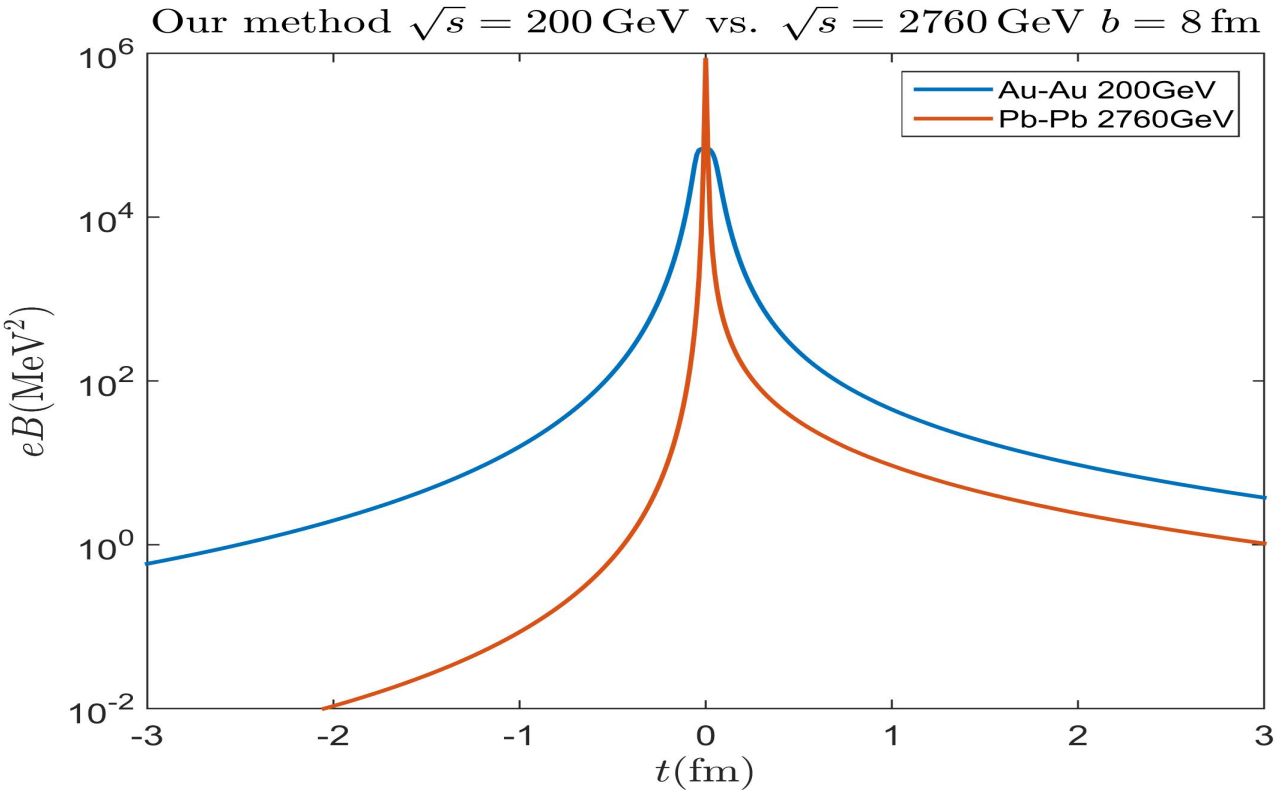

At LHC, magnetic fields falls off rapidly with time than that at RHIC, Chiral Magnetic Effect Is early time dynamics

$$eB\,(\mathrm{t} = 0.2\mathrm{fm}) = 10^3 \sim 10^4\,\mathrm{MeV}^2 \sim 10^{17}\,\mathrm{G} \quad (200\mathrm{GeV})$$

$$eB\,(\mathrm{t} = 0.2\mathrm{fm}) = 10^2 \sim 10^3\,\mathrm{MeV}^2 \sim 10^{16}\,\mathrm{G} \quad (2760\mathrm{GeV})$$

Y. J. Mo, S. Q. Feng and Y. F. Shi, Phys. Rev. C 024901 (2013);
X.Ai and S.Q. Feng, College Physics, 2017, to be published.

Spatial distributions of magnetic field in heavy-ion collisions in the x-z plane

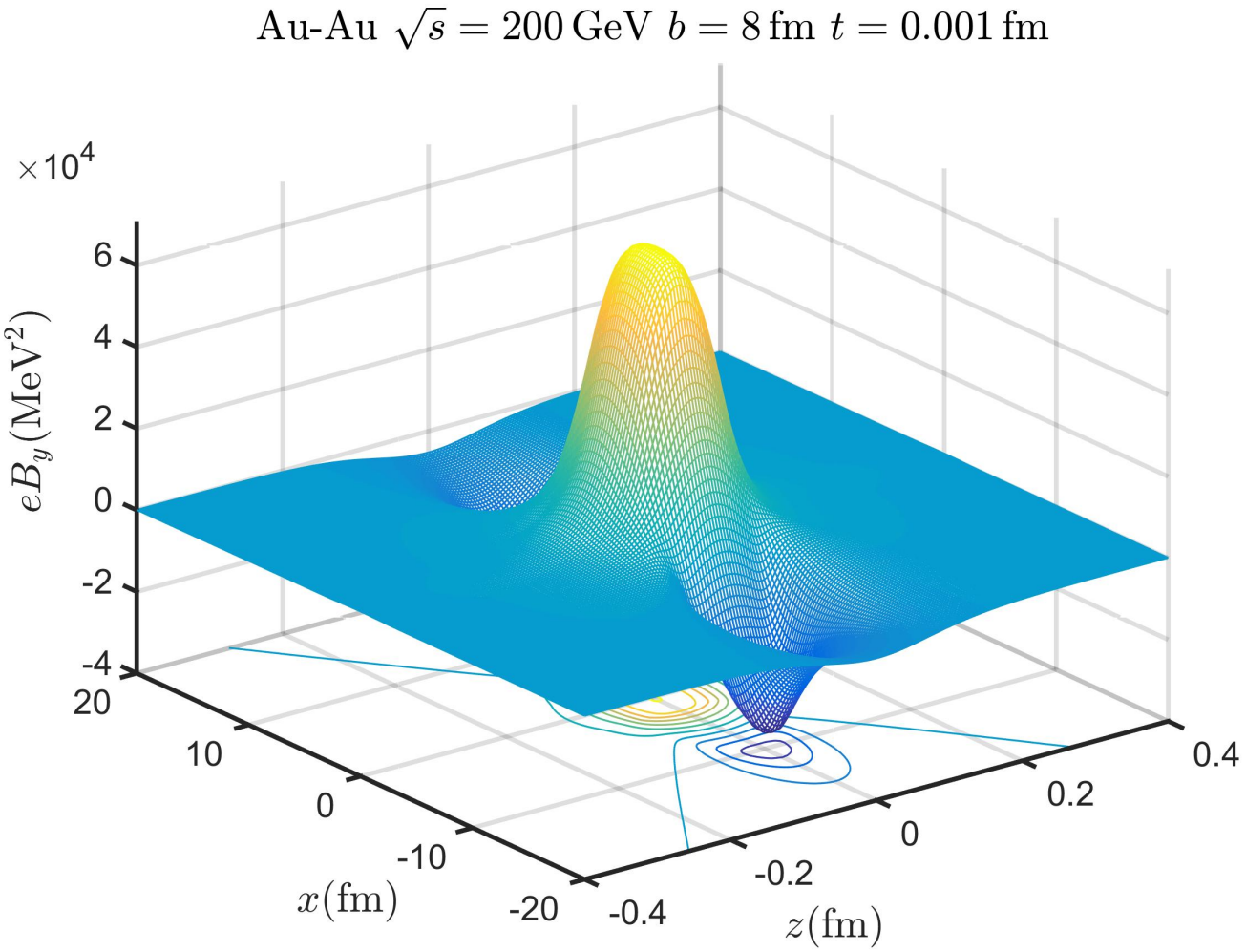

Y. J. Mo, S. Q. Feng and Y. F. Shi, Phys. Rev. C 024901 (2013);
X.Ai and S.Q. Feng, College Physics, 2017, to be published.

Au-Au $\sqrt{s} = 200\,\mathrm{GeV}$ $b = 8\,\mathrm{fm}$ $t = 0.001\,\mathrm{fm}$

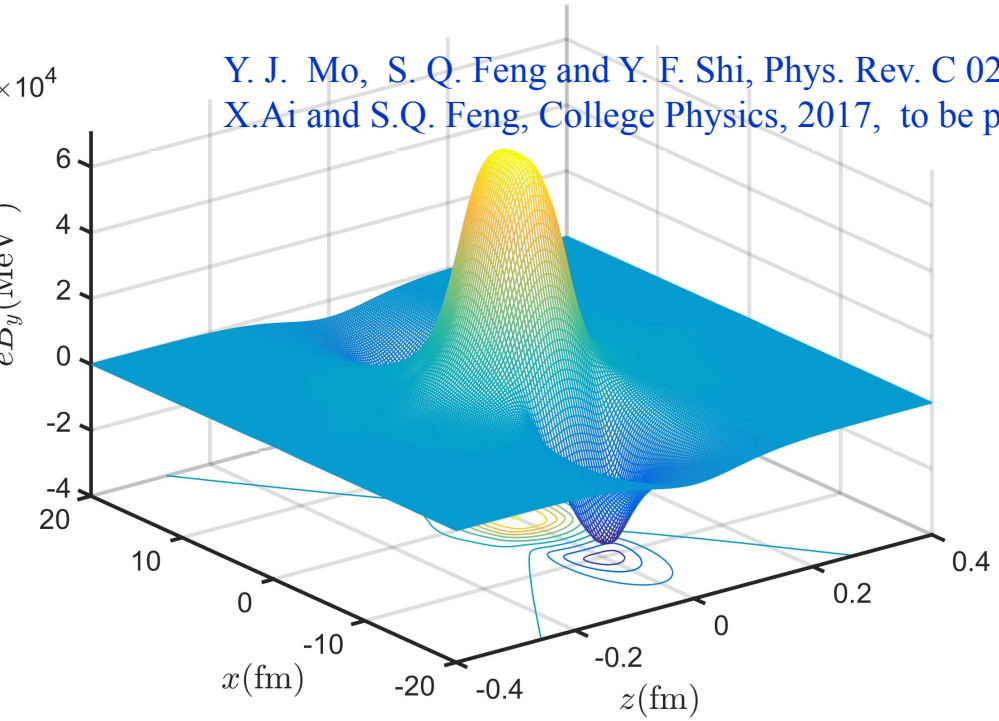

Y. J. Mo, S. Q. Feng and Y. F. Shi, Phys. Rev. C 024901 (2013);
X.Ai and S.Q. Feng, College Physics, 2017, to be published.

Au-Au $\sqrt{s} = 200\,\mathrm{GeV}$ $b = 8\,\mathrm{fm}$ $t = 0.1\,\mathrm{fm}$

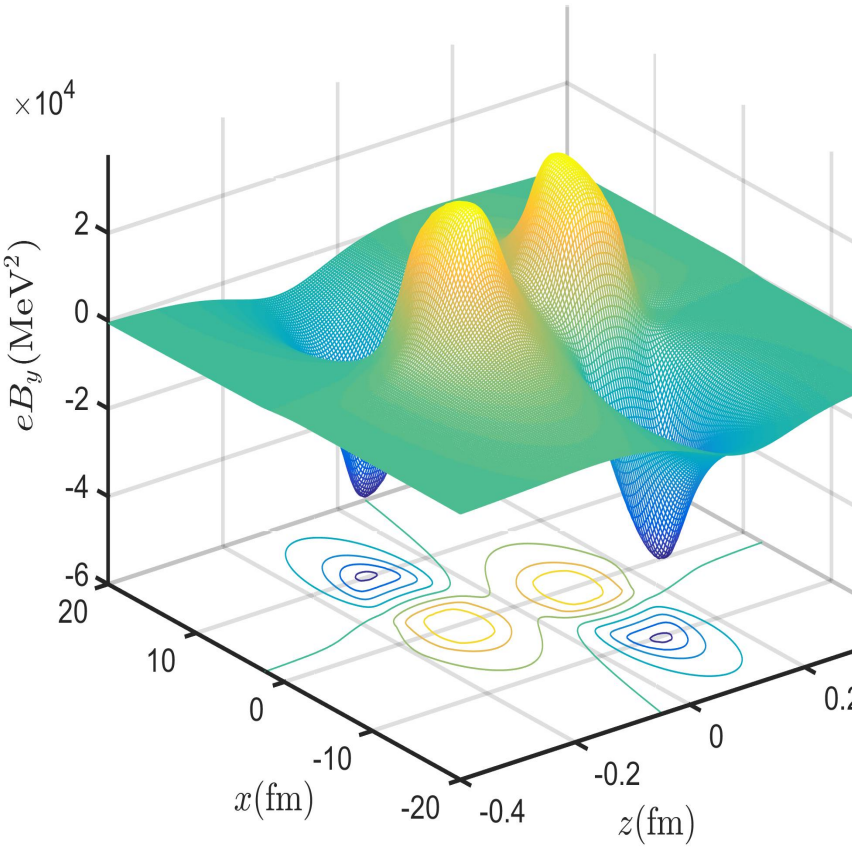

Au-Au $\sqrt{s} = 200\,\mathrm{GeV}$ $b = 8\,\mathrm{fm}$ $t = 0.01\,\mathrm{fm}$

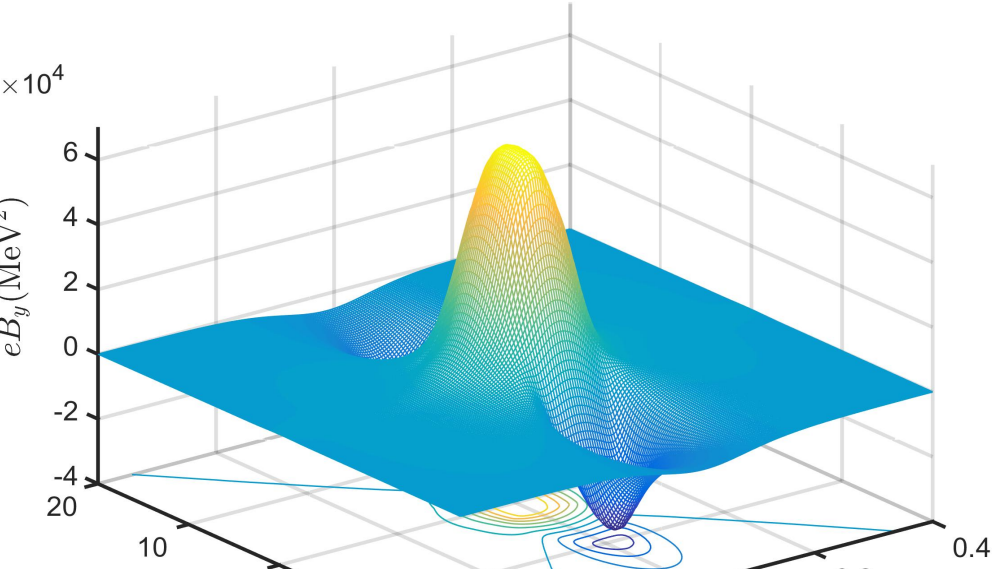

Spatial distributions of magnetic field in heavy-ion collisions in the x-y plane

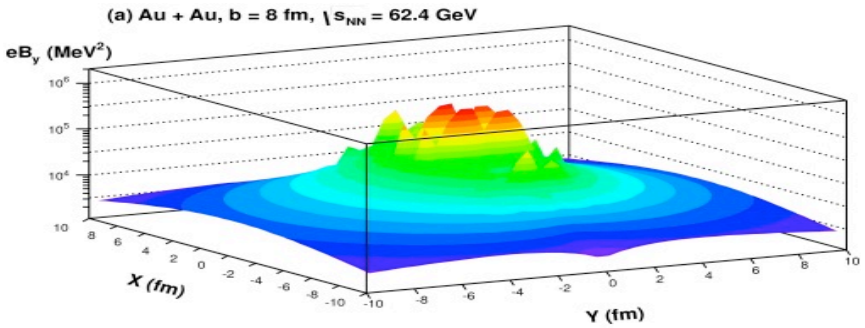

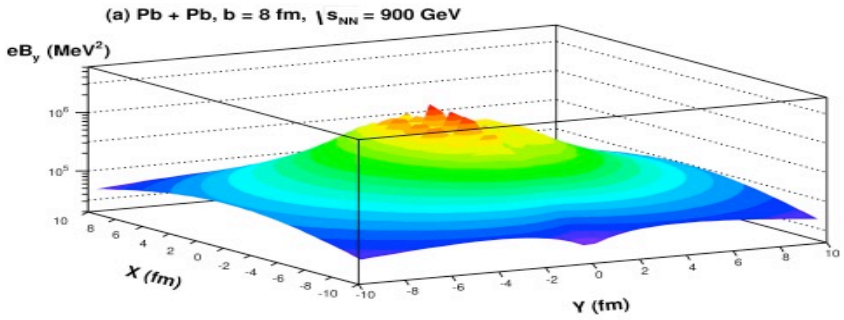

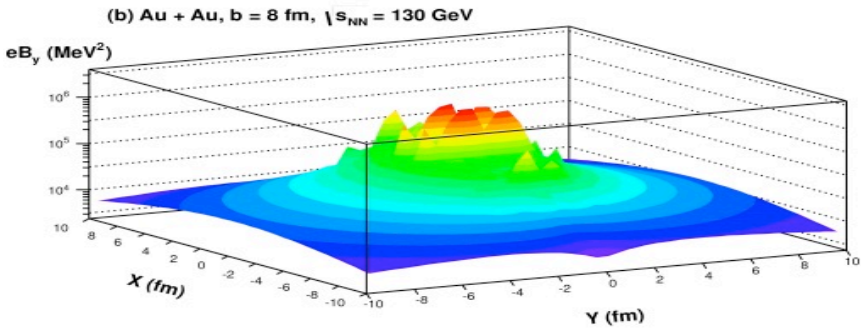

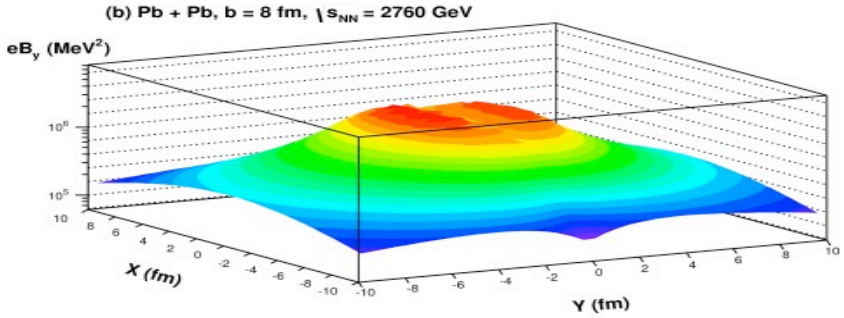

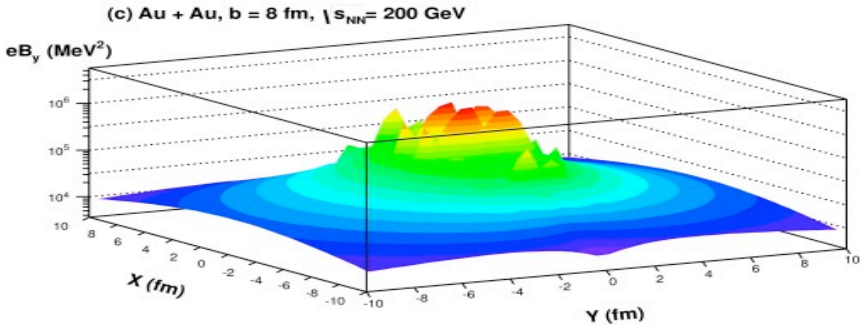

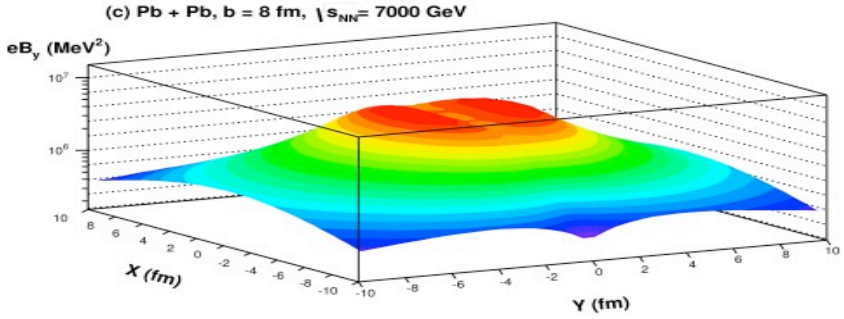

Y. Zhong, C.B.Yang, X.Cai and S.Q. Feng, Advances in High Energy Physics, 1-14(2014)

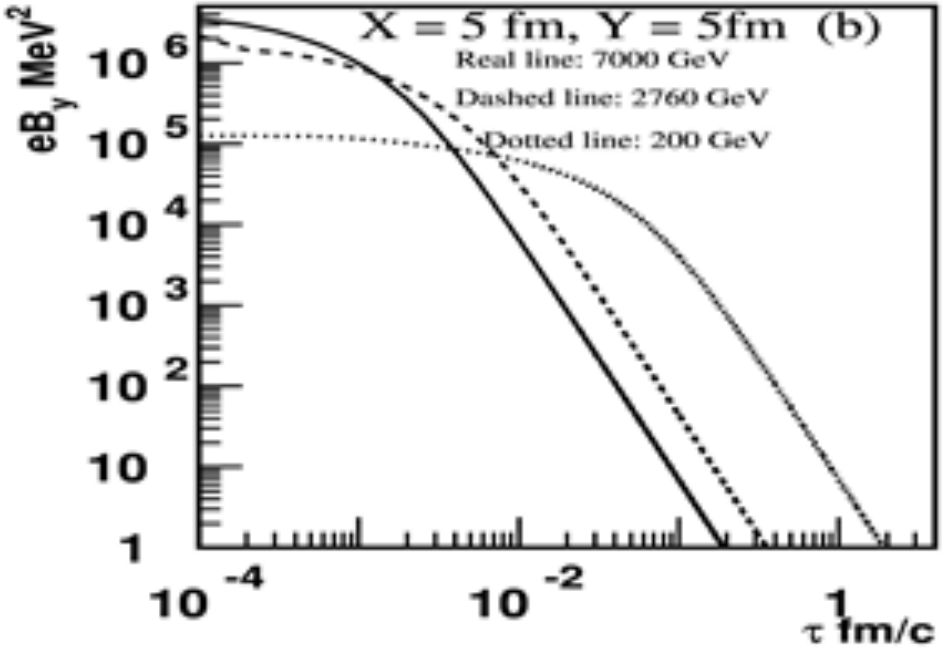

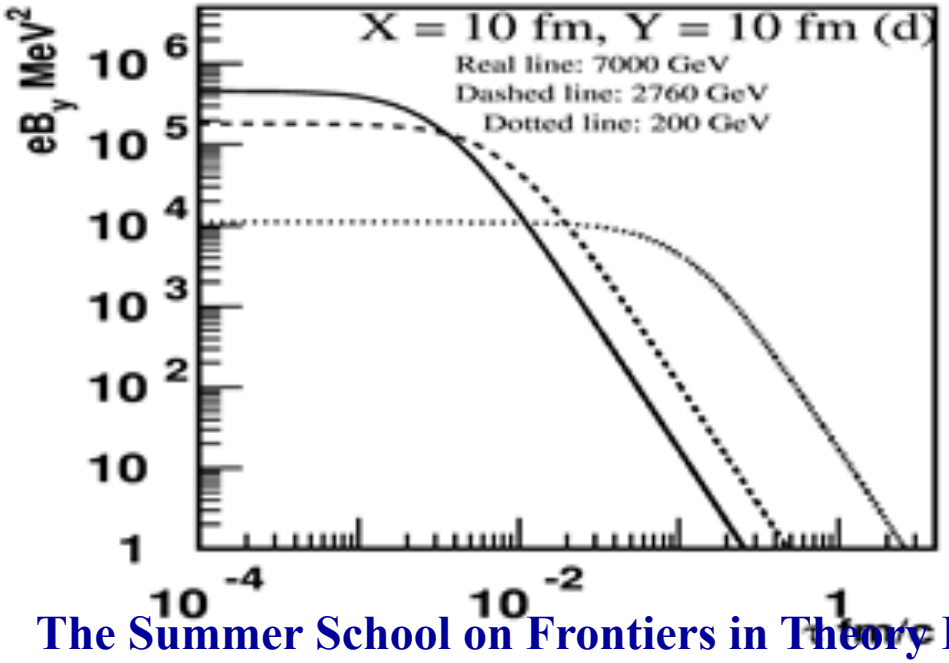

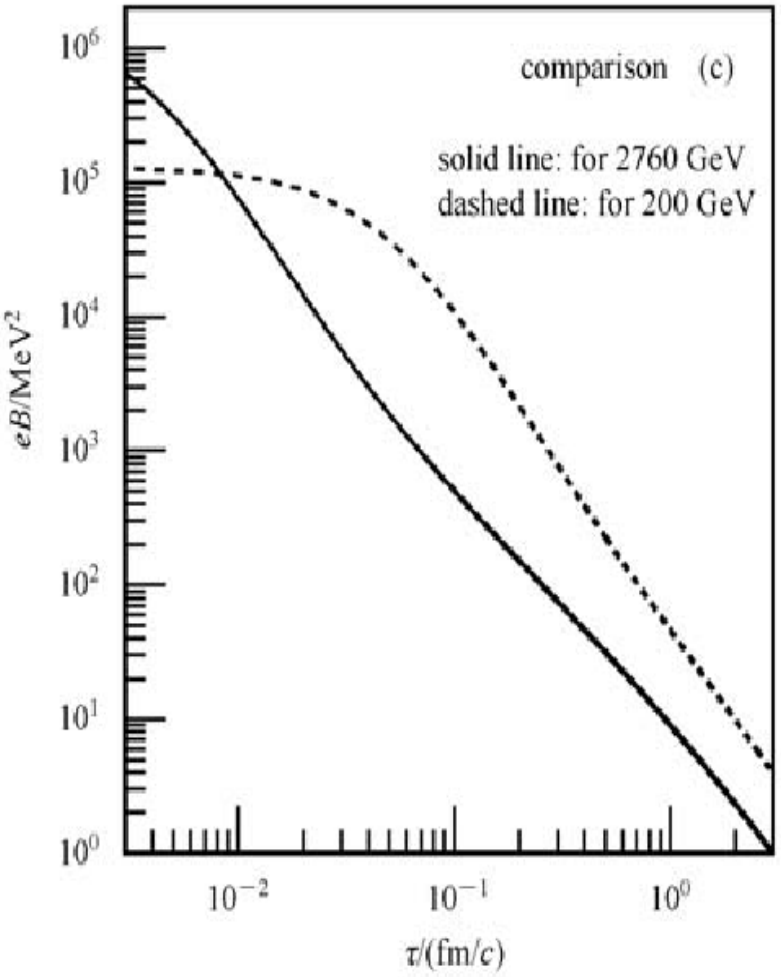

Y. Zhong, C. B. Yang, X. Cai, and S. Q. Fe
Chin. Phys. C39, 104105(2015)

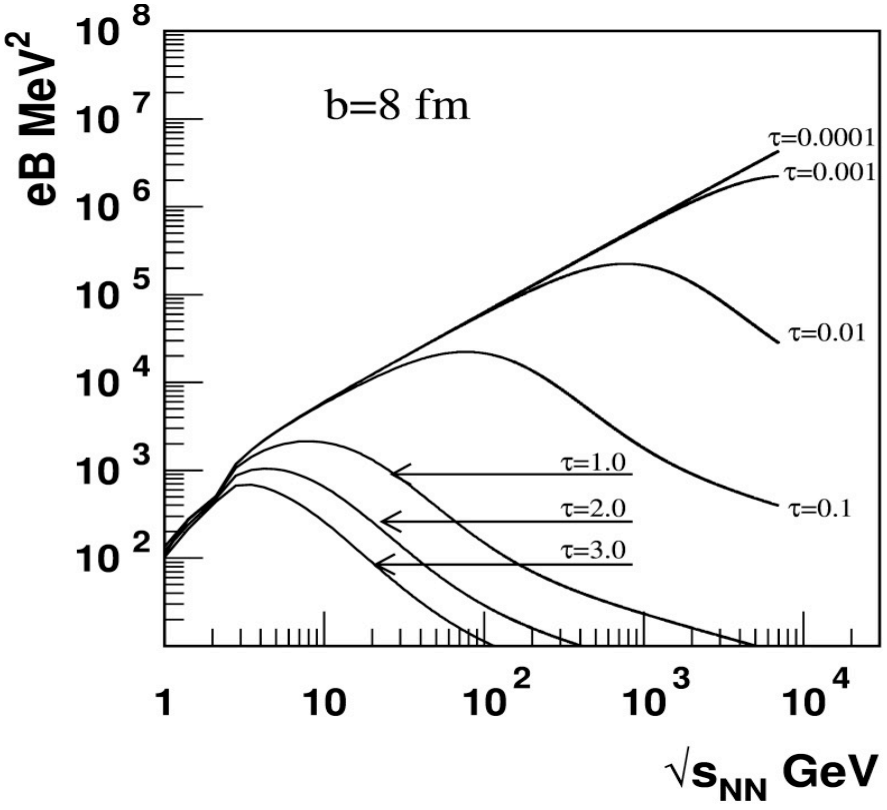

Magnetic fields falls off rapidly：Chiral Magnetic Effect Is early time dynamics

$$eB\,(\mathrm{t}\ = 0.0001\mathrm{fm}) = 10^{6} \sim 10^{7}\,\mathrm{MeV}^{2} \sim 10^{15}\,\mathrm{T}$$

Y. Zhong, C. B. Yang, X. Cai, and S. Q. Feng, Chin. Phys. C39, 104105(2015)

Consider the dependence of magnetic field on the evolution of QGP space-time in relativistic heavy-ion collisions

S.Q. Feng et al.,
arXiv:1609.07550 [nucl-th]

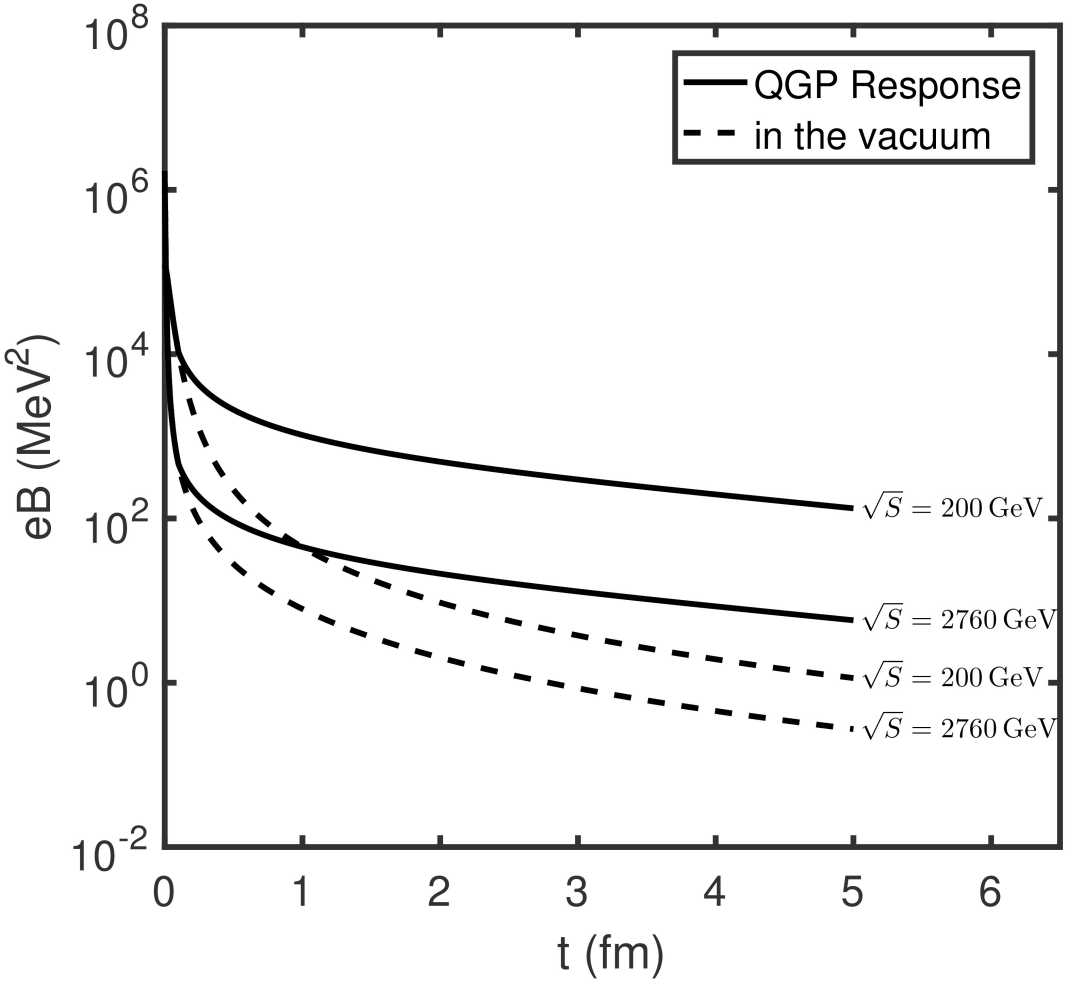

W.T. Deng, and X.G. Huang, Phys. Rev. C85, 044907 (2012)

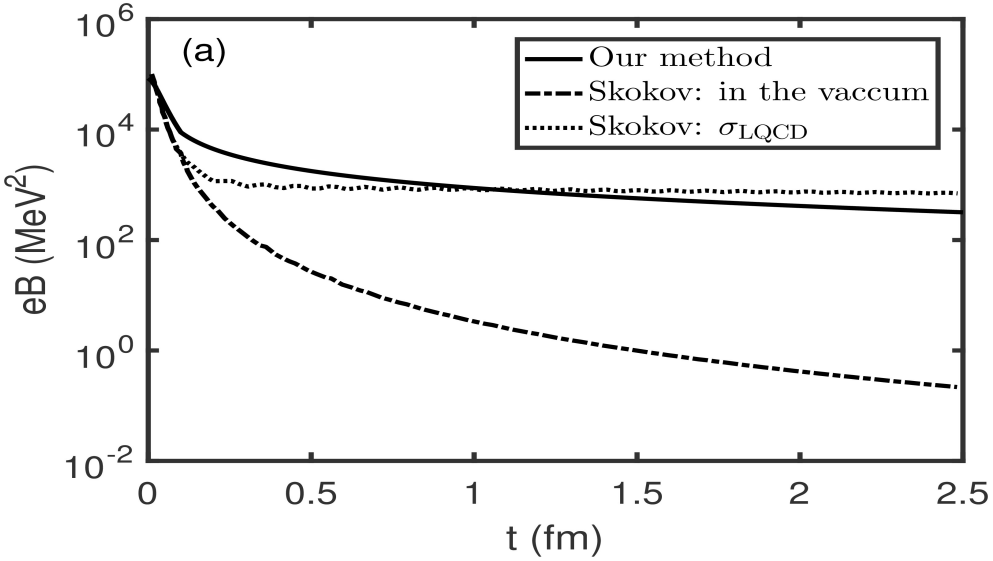
(a)
Our method
Skokov: in the vaccum
Skokov: σ_{LQCD}
eB (MeV^2)
t (fm)

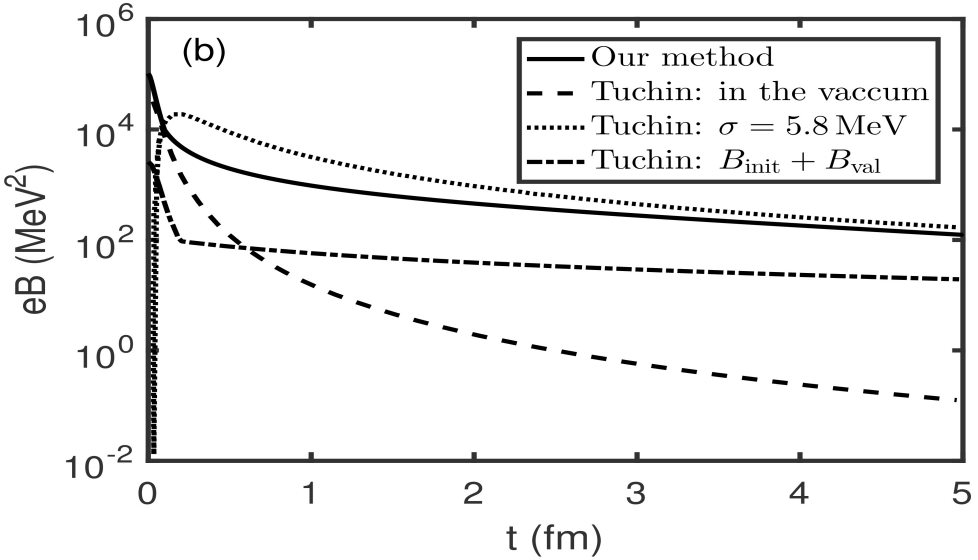
(b)
Our method
Tuchin: in the vaccum
Tuchin: $\sigma = 5.8$ MeV
Tuchin: $B_{\mathrm{init}} + B_{\mathrm{val}}$
eB (MeV^2)
t (fm)

3. Charge Separation features in Relativistic HIC

Chiral Magnetic Effect in Relativistic heavy-Ion Collisions

Non-central nuclear collisions would lead to the asymmetry in the emission of positively and negatively charged particle perpendicular to the reaction plane. Such a charge separation is a consequence of the difference in the number of quarks with positive and negative helicities positioned in the strong magnetic field.

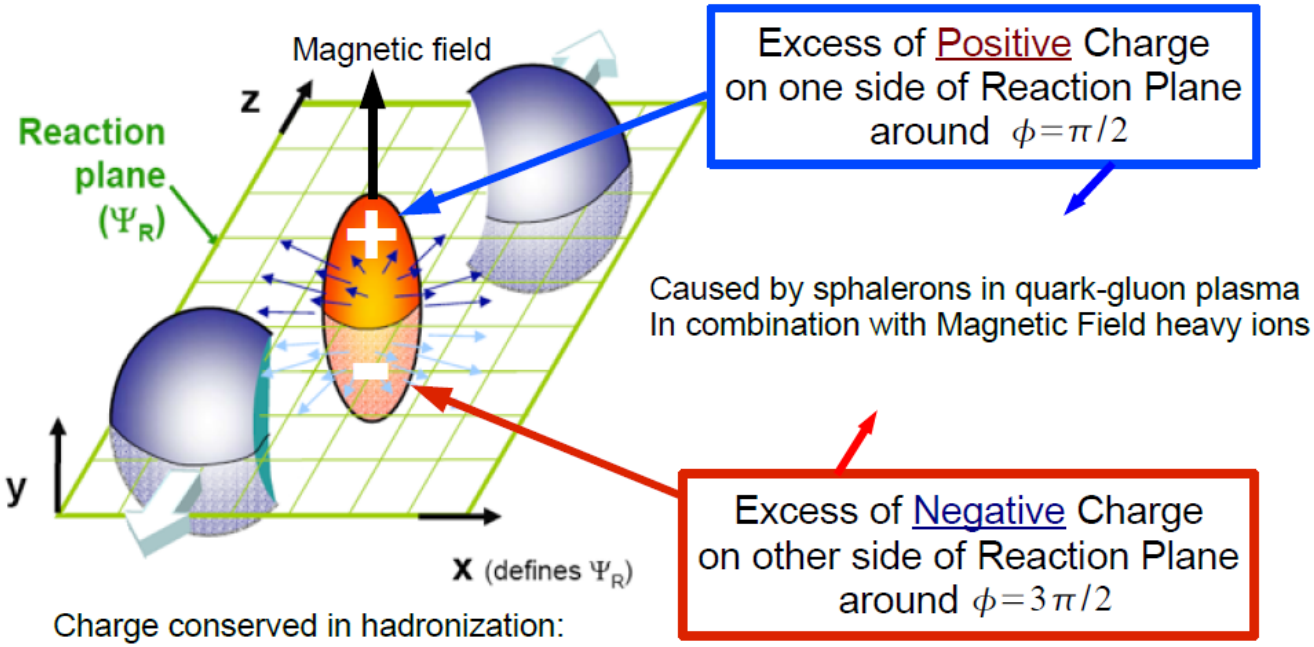

Calculate the charge transtion between both sides of reaction plane

$$\langle \Delta_{\pm}^2 \rangle = 2\int_{t_i}^{t_f} \mathrm{d}t \int_V \mathrm{d}^3x \; \frac{\mathrm{d}N_t}{\mathrm{d}^3x\,\mathrm{d}t} \; [\xi_+^2(x_\perp)+\xi_-^2(x_\perp)] \; \left(\sum_f q_f^2 e B \rho\right)^2$$

Time & Volume integral Overlap region

Rate of Transitions

Screening Functions

Square of Change Charge difference

$$\xi_{\pm}(x_\perp) = \exp\left(-\left|y_{\pm}(x) - y\right|/\lambda\right)$$

$$y_+(x) = -y_-(x) = \begin{cases} \sqrt{R^2-(x-b/2)^2} & -R+b/2 \leqslant x \leqslant 0, \\ \sqrt{R^2-(x+b/2)^2} & 0 \leqslant x \leqslant R-b/2, \end{cases}$$

The Chiral Magnetic Effect is a near the surface effect

Medium causes screening

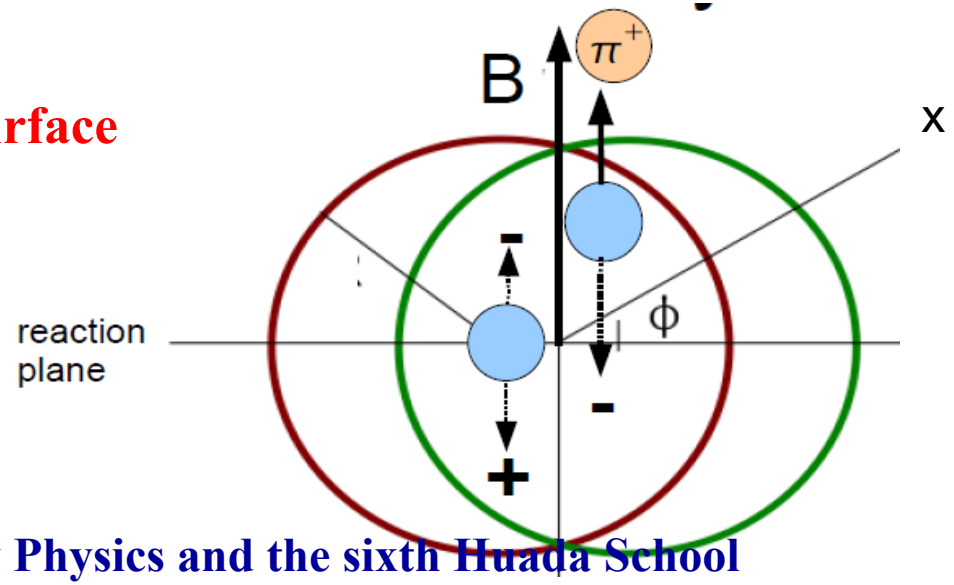

Observables

Voloshin ('04)

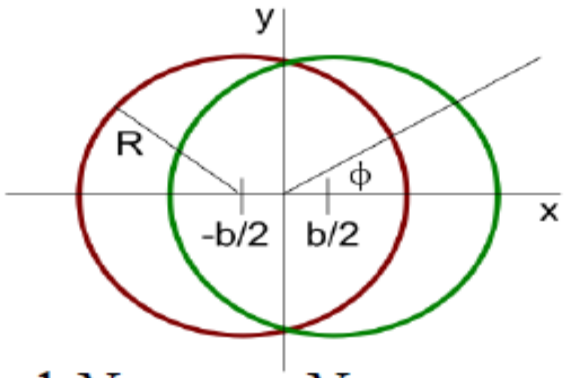

ϕ : angle between particle and reaction plane

$$\frac{dN_{\pm}}{d\phi} = \frac{N_{\pm}}{2\pi} + a_{\pm}\sin\phi + v_2\cos 2\phi + \ldots.$$

Average over many equivalent events (to cancel statistical fluctuations) can give us

$\langle a_+^2 \rangle \sim \langle \Delta_+^2 \rangle$ Pref. emission positive on one side

$\langle a_-^2 \rangle \sim \langle \Delta_-^2 \rangle$ Pref. emission negative on one side

$\langle a_+ a_- \rangle \sim \langle \Delta_+ \Delta_- \rangle$ Correlations between positive on one and negative on other side

Charge Separation features in Relativistic HIC

$$\frac{\mathrm{d}\langle\Delta_{\pm}^2\rangle}{\mathrm{d}\eta} = 2\kappa\alpha_S\left[\sum_f q_f^2\right]^2 \int_{V_\perp} \mathrm{d}^2x_\perp \left[\xi_+^2(x_\perp)+\xi_-^2(x_\perp)\right] \int_{\tau_i}^{\tau_f} \mathrm{d}\tau\,\tau\left[eB(\tau,\eta,x_\perp)\right]^2,$$

$$\frac{\mathrm{d}\langle\Delta_+\Delta_-\rangle}{\mathrm{d}\eta} = -4\kappa\alpha_S\left[\sum_f q_f^2\right]^2 \int_{V_\perp} \mathrm{d}^2x_\perp\, \xi_+(x_\perp)\xi_-(x_\perp) \int_{\tau_i}^{\tau_f} \mathrm{d}\tau\,\tau\left[eB(\tau,\eta,x_\perp)\right]^2,$$

$$a_{++} = a_{--} = \frac{1}{N_+^2}\langle\Delta_{\pm}^2\rangle, \qquad a_{+-} = \frac{1}{N_+N_-}\langle\Delta_+\Delta_-\rangle$$

estimate magnetic asymmetry for large impact parameter 10^{-4}.

$$\xi_{\pm}(x_\perp) = \exp\left(-\left|y_{\pm}(x) - y\right|/\lambda\right)$$

Existence of screening effect

D. Kharzeev, L. D. Mclerran, H. J. Warringa, NPA 803, 227 (2008)

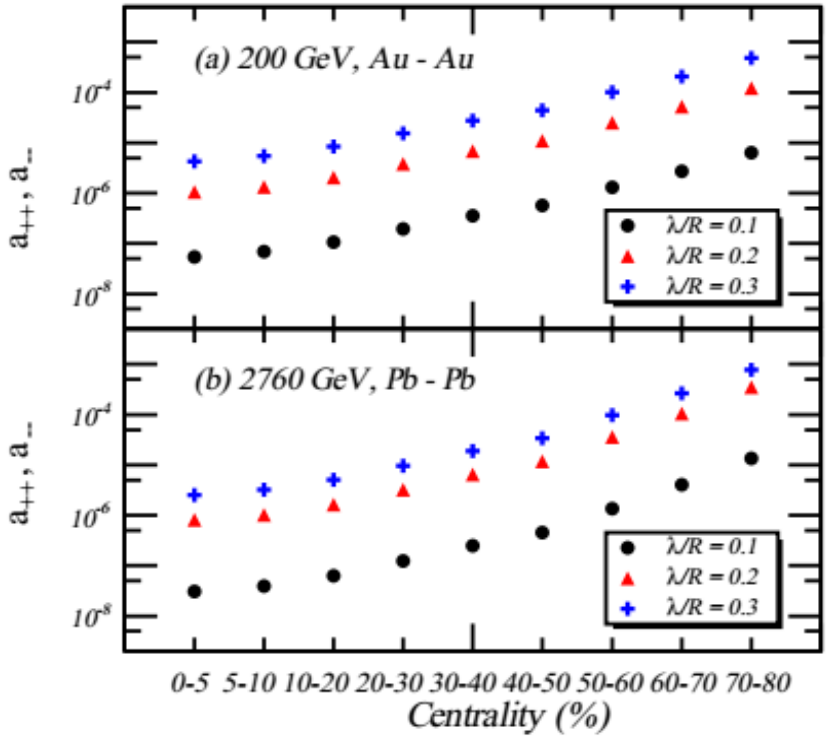

Centrality Dependence of the Charged-Particle Multiplicity Density at Midrapidity in Pb-Pb Collisions at $\sqrt{s_{\mathrm{NN}}} = 2.76$ TeV

K. Aamodt *et al.**
(ALICE Collaboration)

(Received 8 December 2010; published 20 January 2011)

The centrality dependence of the charged-particle multiplicity density at midrapidity in Pb-Pb collisions at $\sqrt{s_{\mathrm{NN}}} = 2.76$ TeV is presented. The charged-particle density normalized per participating nucleon pair increases by about a factor of 2 from peripheral (70%–80%) to central (0%–5%) collisions. The centrality dependence is found to be similar to that observed at lower collision energies. The data are compared with models based on different mechanisms for particle production in nuclear collisions.

DOI: 10.1103/PhysRevLett.106.032301 PACS numbers: 25.75.Gz

Centrality	$dN_{\mathrm{ch}}/d\eta$	$\langle N_{\mathrm{part}} \rangle$
0%–5%	1601 ± 60	382.8 ± 3.1
5%–10%	1294 ± 49	329.7 ± 4.6
10%–20%	966 ± 37	260.5 ± 4.4
20%–30%	649 ± 23	186.4 ± 3.9
30%–40%	426 ± 15	128.9 ± 3.3
40%–50%	261 ± 9	85.0 ± 2.6
50%–60%	149 ± 6	52.8 ± 2.0
60%–70%	76 ± 4	30.0 ± 1.3
70%–80%	35 ± 2	15.8 ± 0.6

Systematic studies of the centrality and $\sqrt{s_{NN}}$ dependence of the $dE_T/d\eta$ and $dN_{ch}/d\eta$ in heavy ion collisions at midrapidity

TABLE XIII. Results of the measurements by PHENIX at $\sqrt{s_{NN}} = 200$ GeV. Errors have the same dimension as the preceding value. Results are plotted in Figs. 5, 7, and 8.

Bin (%)	0–5	5–10	10–15	15–20	20–25	25–30	30–35	35–40	40–45	45–50	50–55	55–60	60–65	65–70
$dN_{ch}/d\eta$	687	560	457	372	302	246	197	156	124	95.3	70.9	52.2	37.5	25.6
Stat. error	0.7	0.6	0.5	0.5	0.4	0.4	0.3	0.3	0.2	0.2	0.2	0.1		
Bending syst. error	25.0	17.0	14.0	11.0	10.0	9.9	9.4	9.0	8.2	7.8	7.1	6.1		4.4
Full syst. error	37.0	28.0	22.0	18.0	16.0	14.0	12.0	11.0	9.6	8.6	7.6	6.5	5.4	4.5

TABLE XIV. Results of the measurements by PHENIX at $\sqrt{s_{NN}} = 130$ GeV. Errors have the same dimension as the preceding value. Results are plotted in Figs. 5, 7, and 8.

Bin (%)	0–5	5–10	10–15	15–20	20–25	25–30	30–35	35–40	40–45	45–50	50–55	55–60	60–65	65–70
$dN_{ch}/d\eta$	602	488	403	329	270	219	176	139	109	84.1	64.3	48.4	35.2	25.3
Stat. error	1.4	1.2	1.1	0.9	0.8	0.7	0.6	0.5	0.4	0.3	0.3	0.3	0.2	0.2
Bending syst. error	19.0	13.0	10.0	9.9	8.6	8.4	8.3	7.7	7.5	6.4	5.9	5.2	4.3	4.1
Full syst. error	28.0	22.0	17.0	15.0	13.0	11.0	10.0	9.1	8.4	7.0	6.3	5.4	4.5	4.1

S.A. Voloshin, Phys. Rev. C 70, 057901 (2004).

$$f(\phi_a, \phi_b) = \frac{1}{N_a N_b} \sum_{i=0}^{N_a} \sum_{j=0}^{N_b} \cos(\phi_{ai} + \phi_{bj}),$$

where $a, b = \pm$ denotes the charge, $N_\pm$ is the total number of positively or negatively charged particles, and ϕ_{ai} denotes the azimuthal angle of an individual charged particle with respect to the reaction plane.

In order toremove the multiplicity fluctuions, one averages the correlators over N_e similar events. The averaging is called event mixing. Voloshin defined the averaged correlators a_{++}(a_{--}) and a_{+-}.

$$a_{ab} = -\frac{1}{N_e} \sum_{n=1}^{N_e} f(\phi_a, \phi_b).$$

$$a_{ab} = -\left\langle \cos(\varphi_a + \varphi_b) \right\rangle$$

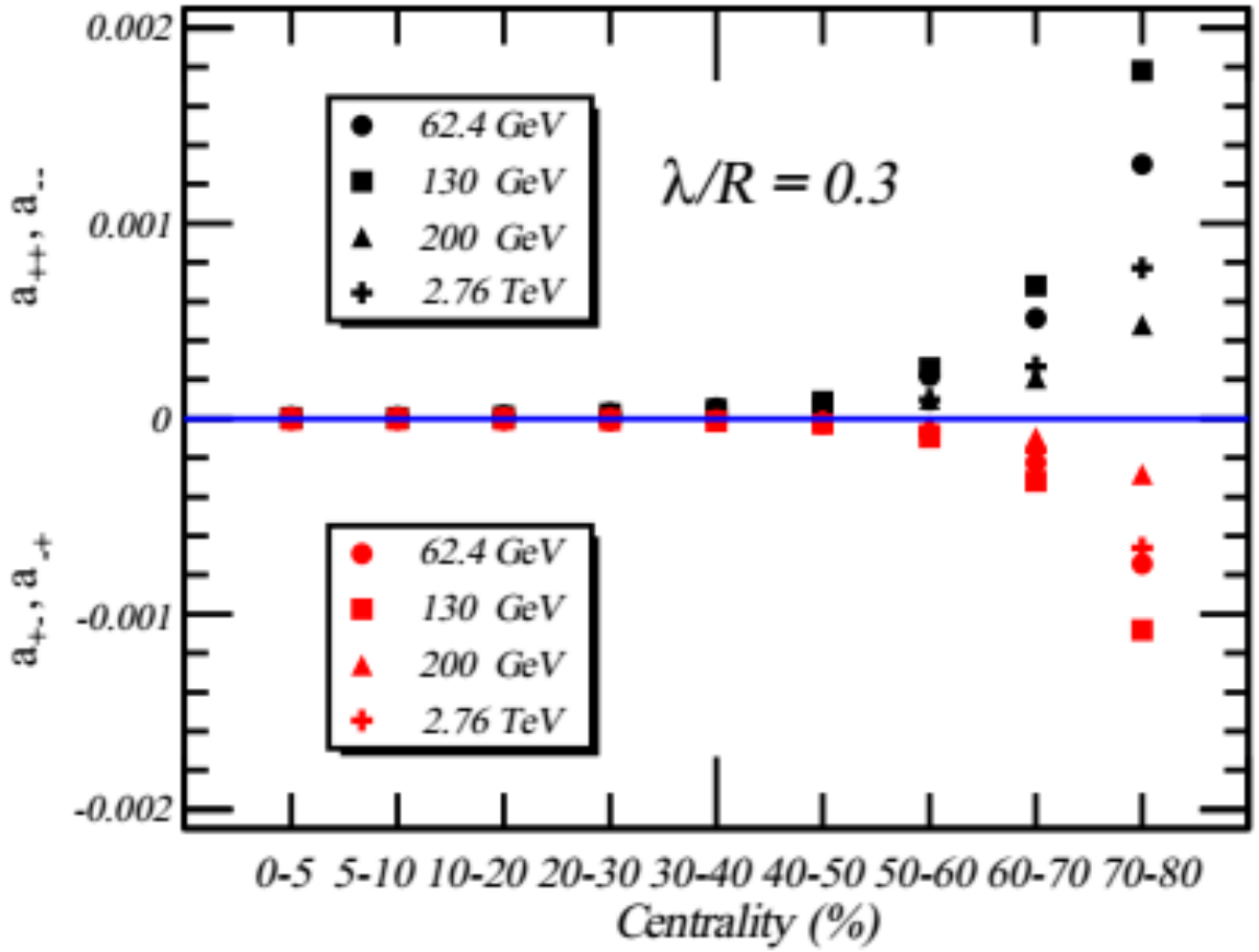

S.Q. Feng et al., arXiv:1609.07550 [nucl-th]

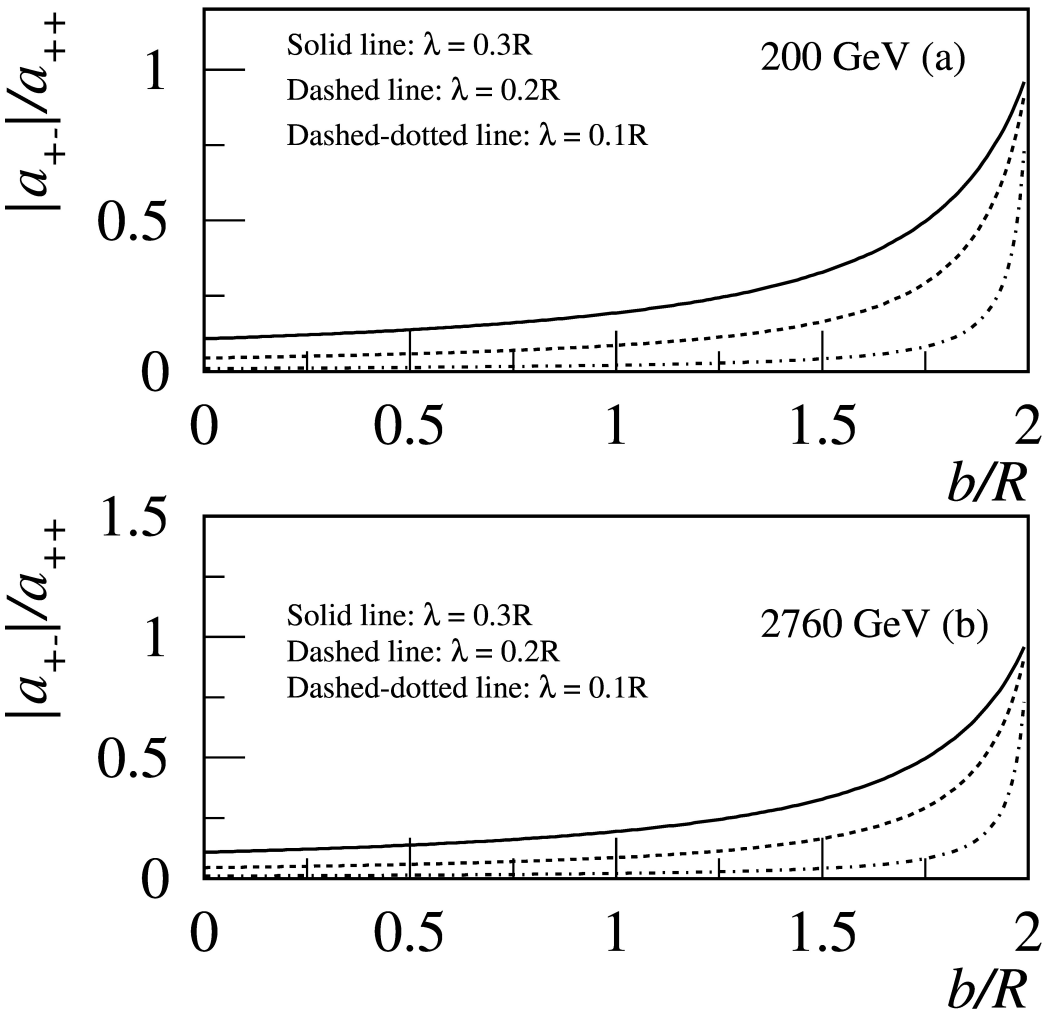

S.Q. Feng et al., arXiv:1609.07550 [nucl-th]

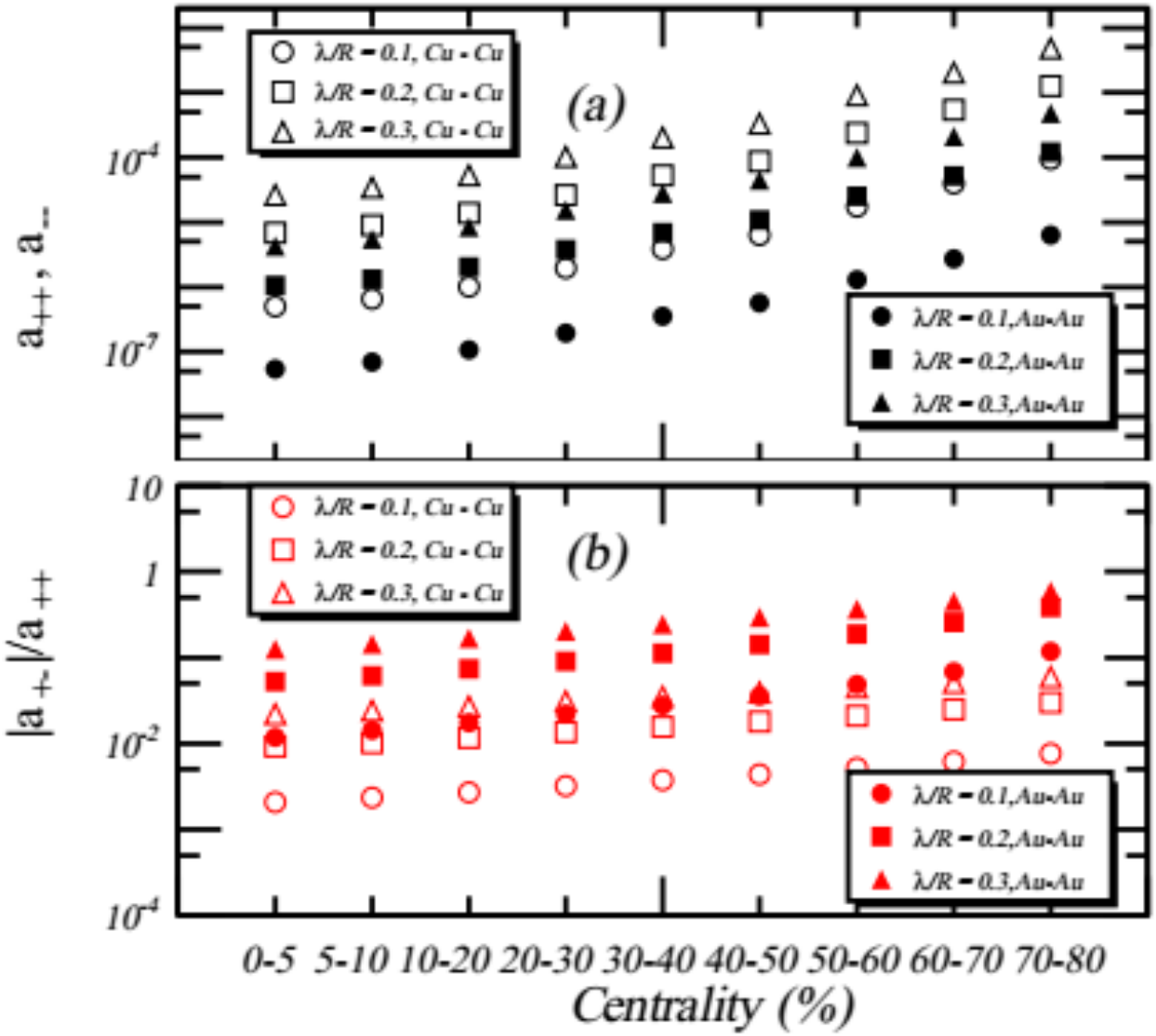
λ/R = 0.1, Cu - Cu
λ/R = 0.2, Cu - Cu
λ/R = 0.3, Cu - Cu
(a)
λ/R = 0.1,Au-Au
λ/R = 0.2,Au-Au
λ/R = 0.3,Au-Au
a_{++}, a_{--}
10^{-4}
10^{-7}
λ/R = 0.1, Cu - Cu
λ/R = 0.2, Cu - Cu
λ/R = 0.3, Cu - Cu
(b)
λ/R = 0.1,Au-Au
λ/R = 0.2,Au-Au
λ/R = 0.3,Au-Au
$|a_{+-}|/a_{++}$
10
1
10^{-2}
10^{-4}
0-5 5-10 10-20 20-30 30-40 40-50 50-60 60-70 70-80
Centrality (%)

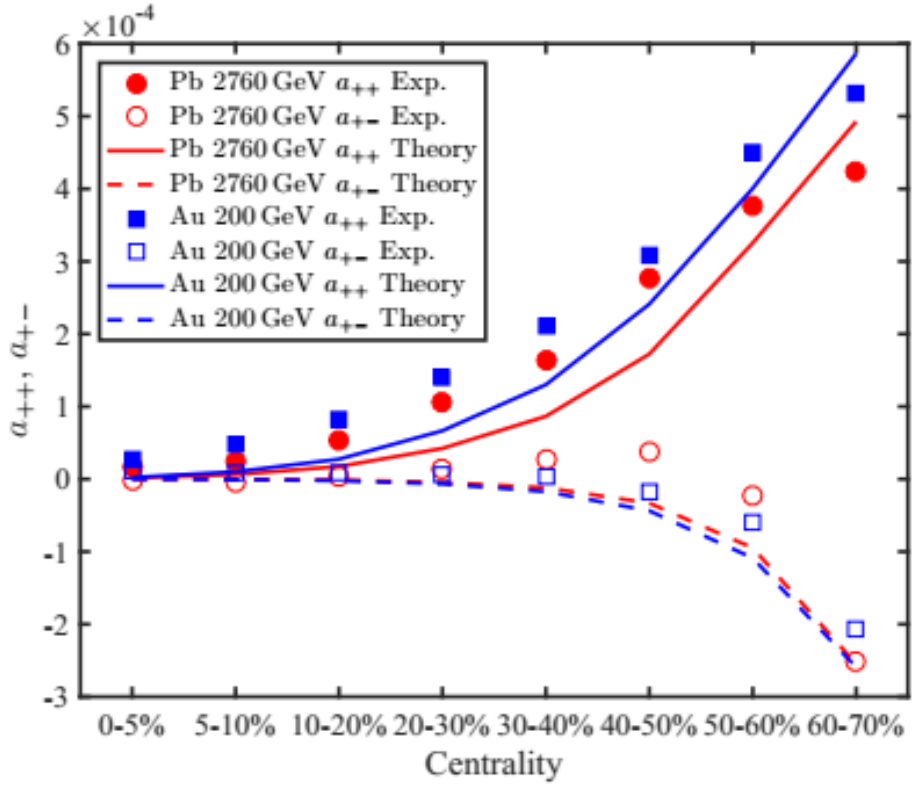
×10^-4
6
5
4
3
2
1
0
-1
-2
-3
a_{++}, a_{+-}
Pb 2760 GeV a_{++} Exp.
Pb 2760 GeV a_{+-} Exp.
Pb 2760 GeV a_{++} Theory
Pb 2760 GeV a_{+-} Theory
Au 200 GeV a_{++} Exp.
Au 200 GeV a_{+-} Exp.
Au 200 GeV a_{++} Theory
Au 200 GeV a_{+-} Theory
0-5%
5-10%
10-20%
20-30%
30-40%
40-50%
50-60%
60-70%
Centrality

Summary and Conclusions

1. By considering the response of the QGP medium in the ideally conducting limit, the magnetic field with the response of QGP medium will maintain a longer time than that of the magnetic field in a vacuum.

2. we calculate the charge separation signal of CME for RHIC and LHC energy region with different centrality. It is found the nuclear screening effect .

3. Magnitude of asymmetry estimate: at large impact parameter

$a_{++} \backsim 1.0*10^{-4}$, The order of magnitude is only 1/4 of the experimental results, but the distribution feature are nearly similar.

Thank your attention

$$\frac{\partial \mathbf{B}}{\partial t} = \nabla \times (\mathbf{v} \times \mathbf{B}) + \frac{1}{\sigma \mu} \left(\nabla^2 \mathbf{B} - \mu \epsilon \frac{\partial^2 \mathbf{B}}{\partial t^2} \right)$$

The first term and the last term on the right-hand sides are the convection terms and the diffusion terms, respectively. The ratio of the first term to the second term is denoted by the magnetic Reynolds number R_m as

$$R_m \equiv LU\sigma\mu$$

Where U is the charateeristic velcity of the flow and L is the characteristic length of time sacle of the QGP. By neglecting the diffusion term , $(\text{taking } R_m \; ? \; 1)$, we take the ideal conducting limit as

$$\frac{\partial \mathbf{B}}{\partial t} = \nabla \times (\mathbf{v} \times \mathbf{B})$$

$$v_z = z / t$$

$$B_y(t, x, y, z) = \frac{t_0}{t} e^{-\frac{c_s^2}{2d_x^2}\left(t^2 - t_0^2\right)} B_y\left(t_0, x_0, y_0, z_0\right)$$

$$\frac{\partial}{\partial t}\mathbf{v}_\perp = -\frac{1}{\varepsilon + P}\nabla_\perp P = -c_s^2 \nabla_\perp \ln \mathfrak{s},$$

where we used $\varepsilon + P = T\mathfrak{s}$, $\mathfrak{s}$ is the entropy density, and $c_s = \sqrt{\partial P/\partial \varepsilon}$ is the speed of sound. For simplicity, we choose an initial Gaussian transverse entropy density profile

$$\mathfrak{s}(x, y) = \mathfrak{s}_0 \exp\left(-\frac{x^2}{2a_x^2} - \frac{y^2}{2a_y^2}\right)$$

$$v_x = \frac{c_s^2}{a_x^2} x t,$$

$$v_y = \frac{c_s^2}{a_y^2} y t.$$

$$B_x(t, x, y, z) = \frac{t_0}{t} e^{-\frac{c_s^2}{2a_y^2}(t^2 - t_0^2)} \times B_x^0\left(x e^{-\frac{c_s^2}{2a_x^2}(t^2 - t_0^2)}, y e^{-\frac{c_s^2}{2a_y^2}(t^2 - t_0^2)}, z\frac{t_0}{t}\right),$$

$$B_y(t, x, y, z) = \frac{t_0}{t} e^{-\frac{c_s^2}{2a_x^2}(t^2 - t_0^2)} \times B_y^0\left(x e^{-\frac{c_s^2}{2a_x^2}(t^2 - t_0^2)}, y e^{-\frac{c_s^2}{2a_y^2}(t^2 - t_0^2)}, z\frac{t_0}{t}\right)$$

$$x = x_0 \exp\left[\frac{c_s^2}{2a_x^2}(t^2 - t_0^2)\right],$$

$$y = y_0 \exp\left[\frac{c_s^2}{2a_y^2}(t^2 - t_0^2)\right],$$

$$z = z_0 \frac{t}{t_0}.$$

$$B_x(t,x,y,z) = \frac{t_0}{t} e^{-\frac{c_s^2}{2d_y^2}\left(t^2 - t_0^2\right)} B_x\left(t_0, x_0, y_0, z_0\right)$$

$$B_y(t,x,y,z) = \frac{t_0}{t} e^{-\frac{c_s^2}{2d_x^2}\left(t^2 - t_0^2\right)} B_y\left(t_0, x_0, y_0, z_0\right)$$

$$\rho_\pm(\boldsymbol{x}') = \frac{\gamma n_0}{1+\exp\left(\frac{\sqrt{(x'\pm b/2)^2+y'^2+(\gamma z')^2}-R}{d}\right)}.$$

$$e\boldsymbol{B}_s^\pm(t,\boldsymbol{x}) = \pm Z\alpha_{\mathrm{EM}}\sinh Y_0 \int_{V_s^\pm} \mathrm{d}^3\boldsymbol{x}'\,\rho_\pm(\boldsymbol{x}') \times \frac{(\boldsymbol{x}'_\perp-\boldsymbol{x}_\perp)\times\boldsymbol{e}_z}{[(\boldsymbol{x}'_\perp-\boldsymbol{x}_\perp)^2+((\frac{z'}{\tanh Y_0}\pm t)\sinh Y_0 - z\cosh Y_0)^2]^{3/2}}$$

$$e\boldsymbol{B}_p^\pm(t,\boldsymbol{x}) = \pm Z\alpha_{\mathrm{EM}} \int_{V_p} \mathrm{d}^3\boldsymbol{x}' \int_{-Y_0}^{Y_0} \mathrm{d}Y\, f(Y)\sinh Y\,\rho_\pm(\boldsymbol{x}') \times \frac{(\boldsymbol{x}'_\perp-\boldsymbol{x}_\perp)\times\boldsymbol{e}_z}{[(\boldsymbol{x}'_\perp-\boldsymbol{x}_\perp)^2+((\frac{z'}{\tanh Y_0}\pm t)\sinh Y - z\cosh Y)^2]^{3/2}}$$

$$\boldsymbol{B} = \boldsymbol{B}_s^+ + \boldsymbol{B}_s^- + \boldsymbol{B}_p^+ + \boldsymbol{B}_p^-$$